

# USING OPAQUE IMAGE BLUR FOR REAL-TIME DEPTH-OF-FIELD RENDERING

Martin Kraus

*Department of Architecture, Design and Media Technology, Aalborg University  
Niels Jernes Vej 14, 9220 Aalborg Øst, Denmark*

**Keywords:** Depth of field, Blur, Glow, Visual effect, Real-time rendering, Image processing, GPU, Pyramid algorithm.

**Abstract:** While depth of field is an important cinematographic means, its use in real-time computer graphics is still limited by the computational costs that are necessary to achieve a sufficient image quality. Specifically, color bleeding artifacts between objects at different depths are most effectively avoided by a decomposition into sub-images and the independent blurring of each sub-image. This decomposition, however, can result in rendering artifacts at silhouettes of objects. While various algorithms have been suggested to eliminate these artifacts, we propose a new blur filter that increases the opacity of all pixels to avoid artifacts at the cost of physically less accurate but still plausible rendering results. The proposed filter is named “opaque image blur” and is based on a glow filter that is applied to the alpha channel. We present a highly efficient GPU-based pyramid algorithm that implements this filter for depth-of-field rendering.

## 1 INTRODUCTION

Depth of field in photography specifies the depth range of the region in front and behind the focal plane that appears to be in focus for a given resolution of the film. As limited depth of field is a feature of all real camera systems (including the human eye), plausible depth-of-field effects can significantly enhance the illusion of realism in computer graphics. Moreover, limited depth of field can be used to guide the attention of viewers. In fact, it is routinely used for this purpose in movies — including computer-animated movies. In recent years, it has also been used in several computer games and first applications in graphical user interfaces have been demonstrated.

There are various approaches to the computation of depth-of-field effects, which provide different trade-offs between image quality and rendering performance. Current techniques for real-time performance are based on a single pinhole image with infinite depth of field since the performance of this approach is independent of the scene complexity and graphics hardware is optimized to compute this kind of imagery. One of the most prominent rendering artifacts in this approach is color bleeding between objects at different depths.

One way to avoid these particular artifacts is the decomposition of the pinhole image into sub-images

according to the depth of pixels and the independent processing of each sub-image. The main remaining artifact is caused by partial occlusions. More specifically, the problem is caused by pixels of one sub-image that are occluded by the pinhole version of another sub-image in the foreground but only partially occluded by the blurred version of that sub-image. Various approaches have been suggested to address these disoccluded pixels; however, all proposed methods tend to be the most costly part of the respective algorithm in terms of rendering performance.

In this work, we solve the problem by completely avoiding disocclusions of pixels; i.e., instead of trying to render correct images with disoccluded pixels, we render plausible images without disoccluded pixels. The key element of our approach is a blurring method that does not disocclude pixels; i.e., a blur filter that does not reduce the opacity of any pixel. This filter allows us to design a considerably simplified algorithm for sub-image blurring, which is presented in Section 3. The details of the employed blurring method — named “opaque image blur” — are discussed in Section 4. Results are presented in Section 5 while conclusions and plans for future work are discussed in Sections 6 and 7. First, however, we discuss previous work.

## 2 PREVIOUS WORK

Physically correct depth-of-field effects in off-line rendering are most commonly computed by stochastic sampling of a camera lens of finite size (Cook et al., 1984). Several implementations with various improvements have been published (Cook et al., 1987; Haeberli and Akeley, 1990; Kolb et al., 1995; Pharr and Humphreys, 2004; Lee et al., 2010).

Splatting of image points with the help of a depth-dependent point-spread function was proposed even earlier than stochastic sampling (Potmesil and Chakravarty, 1982) and can also produce accurate images if all points of a scene are taken into account (including points that are occluded in a pinhole image). While the first implementations were software-based (Shinya, 1994; Křivánek et al., 2003), more recent systems employ features of modern graphics hardware (Lee et al., 2008).

The principle drawback of stochastic sampling and splatting approaches with respect to performance is the dependency on the scene complexity, i.e., the rendering of the depth-of-field effect is more costly for more complex scenes. Furthermore, the computations have to be integrated into the rendering process and, therefore, often conflict with optimizations of the rendering pipeline, in particular in the case of hardware-based pipelines. Therefore, real-time and interactive approaches to depth-of-field rendering are based on image post-processing of pinhole images with depth information for each pixel. These approaches are independent of the scene complexity and they are compatible with any rendering method that produces pinhole images with depth information.

The highest performance is achieved by computing a series of differently blurred versions (e.g., in the form of a mipmap hierarchy) and determining an appropriately blurred color for each pixel based on these filtered versions (Rokita, 1993; Demers, 2004; Hammon, 2007; Lee et al., 2009b). However, it appears to be impossible to avoid all rendering artifacts in these approaches — in particular color bleeding (also known as intensity leakage) between objects at different depths.

The most effective way to avoid these artifacts is the decomposition of the pinhole image into sub-images according to the depth of pixels (Barsky, 2004). Each sub-image is then blurred independently and the blurred sub-images are blended onto each other to accumulate the result. However, the decomposition into sub-images can introduce new artifacts at the silhouettes of sub-images, which are addressed in different ways by the published systems (Barsky et al., 2005; Kraus and Strengert, 2007a).

Hybrid approaches are also possible; in particular, the scene geometry can be rendered into different layers which are then blurred independently (Scofield, 1992; Kosloff and Barsky, 2007; Kosloff et al., 2009; Lee et al., 2009a). This can avoid artifacts between layers but requires non-uniform blurring techniques, which require a considerably higher performance.

This work is based on the system presented by Kraus and Strengert but eliminates artifacts at silhouettes by avoiding partial disocclusions of pixels. This is achieved by employing a particular blur filter, which does not reduce the opacity of any pixel. Thus, the effect is similar to applying a glow filter (James and O’Rorke, 2004) to the opacity channel. In principle, a grayscale morphological filter (Sternberg, 1986) could also be used for this purpose; however, the GPU-based computation of glow filters offers a considerably higher performance.

## 3 DEPTH-OF-FIELD RENDERING

The proposed algorithm decomposes a pinhole image with depth information into sub-images that correspond to certain depth ranges as illustrated in Figure 1. Similarly to previously published methods (Barsky et al., 2005; Kraus and Strengert, 2007a), the algorithm consists of a loop over all sub-images starting with the sub-image corresponding to the farthest depth range. For each sub-image, the following three steps are performed:

1. The pinhole image is matted according to the pixels’ depth (Figure 1c).
2. The matted sub-image is blurred using the “opaque image blur” discussed in Section 4 (Figure 1d).
3. The blurred sub-image is blended over the content of an (initially cleared) framebuffer, in which the result is accumulated (Figure 1f).

Note that no disocclusion of pixels is necessary whereas the disocclusion step in previous published systems tends to be the most costly computation (Barsky et al., 2005; Kraus and Strengert, 2007a).

The matting and blending in our prototype is performed as in the system by Kraus and Strengert. Specifically, we approximate the blur radius  $r_i$  of the  $i$ -th sub-image by:

$$r_i \stackrel{\text{def}}{=} 1.7 \times 2^{|i|-1} \text{ for } i \neq 0 \text{ and } r_0 \stackrel{\text{def}}{=} 0. \quad (1)$$

The blur radius is specified in pixels and corresponds to the radius of the circle of confusion. Thus, the corresponding depth  $z_i$  of the  $i$ -th sub-image can be com-

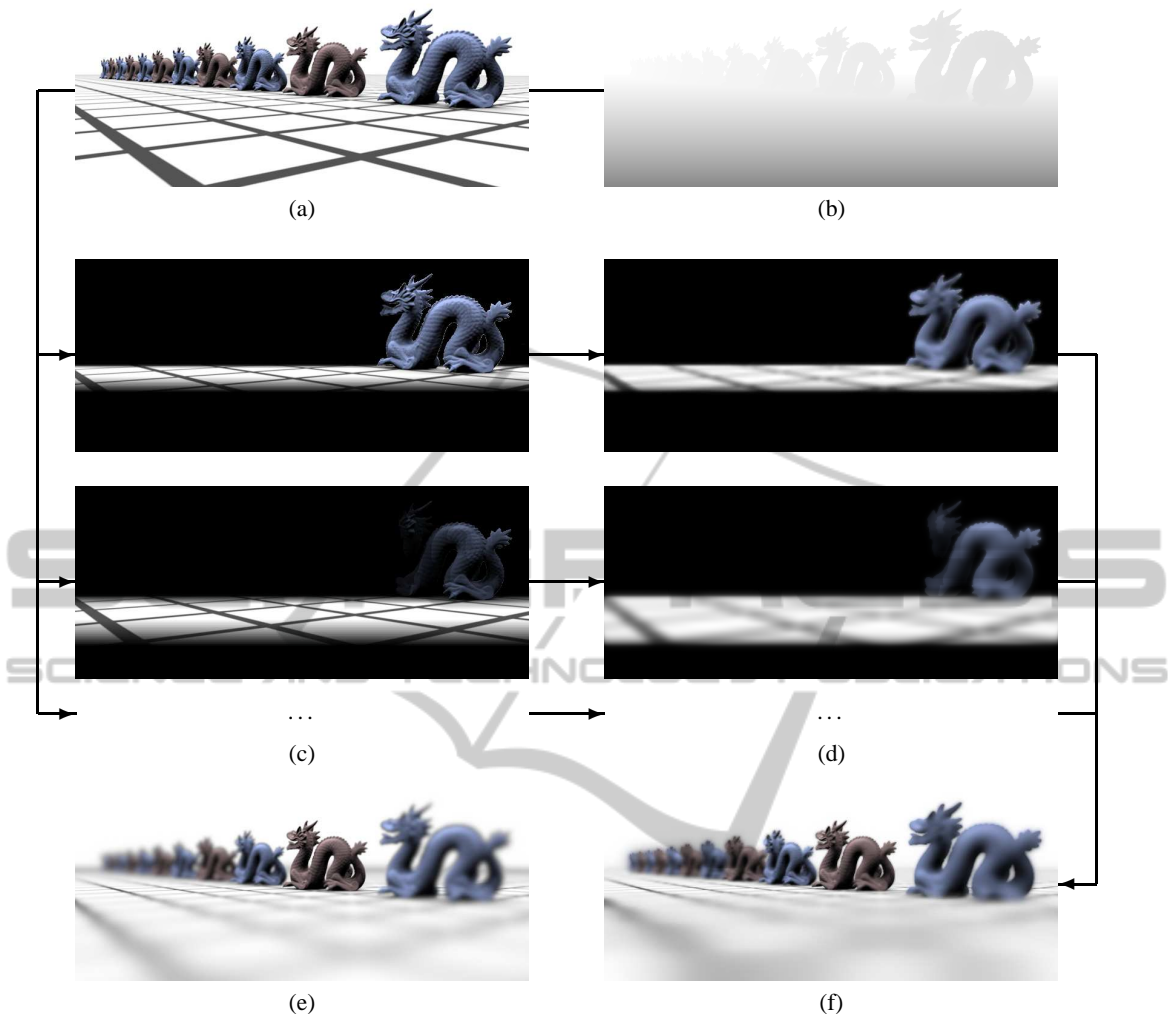


Figure 1: Data flow in our method: (a) input pinhole image, (b) input depth map, (c) sub-images after matting, (d) sub-images after opaque image blur (see Figure 3), (e) ray-traced reference image (Pharr and Humphreys, 2004), (f) blended result of our method. In (c) and (d) only the opacity-weighted RGB components of the  $(-1)$ st sub-image (*top*) and the  $(-2)$ nd sub-image (*bottom*) are shown.

puted with the thin lens approximation. The result is:

$$z_i \stackrel{\text{def}}{=} \frac{z_{\text{focal}}}{1 + r_i/r_\infty} \quad \text{for } i < 0, \quad (2)$$

$$z_0 \stackrel{\text{def}}{=} z_{\text{focal}}, \quad (3)$$

$$z_i \stackrel{\text{def}}{=} \frac{z_{\text{focal}}}{1 - r_i/r_\infty} \quad \text{for } i > 0. \quad (4)$$

Here,  $z_{\text{focal}}$  is the depth of the focal plane and  $r_\infty$  is the blur radius of infinitely distant points.  $r_\infty$  can be expressed in terms of the focal length  $f$ , the f-number  $N$ , the field-of-view angle in y direction  $\gamma_{\text{fovy}}$ , and the height of the image  $h_{\text{pix}}$  in pixels:

$$r_\infty \stackrel{\text{def}}{=} \frac{h_{\text{pix}}}{2z_{\text{focal}} \tan(\gamma_{\text{fovy}}/2)} \frac{f}{2N}. \quad (5)$$

The depths  $z_{i-2}$ ,  $z_{i-1}$ ,  $z_i$ , and  $z_{i+1}$  of four sub-images are used to define the matting functions  $\omega_i(z)$  for pixels of the  $i$ -th sub-image as illustrated in Figure 2. However, the weighting functions for the foremost and backmost sub-images are adjusted to remove the ramps at the extremes; i.e., the weight is set to 1 where there is no other sub-image that would include a pixel.

The matting of the  $i$ -th sub-image is then performed in a fragment shader by looking up the depth  $z$  of each pixel, evaluating the weighting function  $\omega_i(z)$  and multiplying it to the RGBA color of the pinhole image, where the opacity  $A$  of the pinhole image is set to 1.

After matting, each sub-image is blurred as described in Section 4. The resulting blurred colors  $\text{RGBA}_{\text{sub}}$  of the sub-image are then blended with the

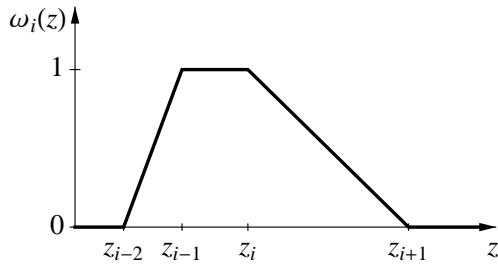


Figure 2: Illustration of the matting function  $\omega_i(z)$  for the  $i$ -th sub-image based on the depths  $z_{i-2}$  to  $z_{i+1}$ .

colors  $RGB_{buf}$  of a color buffer, which is initially set to black. The blending employs the “over” operator for pre-multiplied (i.e., opacity-weighted) colors (Porter and Duff, 1984) since the sub-images are processed from back to front:

$$RGB_{buf} \leftarrow RGB_{sub} + (1 - A_{sub}) \times RGB_{buf}. \quad (6)$$

After the frontmost sub-image has been processed, the colors  $RGB_{buf}$  represent the resulting image with the computed depth-of-field effect.

While this algorithm is significantly less complex than previously published algorithms for sub-image processing (Barsky et al., 2005; Kraus and Strengert, 2007a), it strongly depends on an image blur that does not disocclude pixels, i.e., the image blur must not decrease the opacity of any pixel. The next section describes such a filter.

## 4 OPAQUE IMAGE BLUR

The proposed “opaque image blur” of sub-images guarantees not to disocclude pixels in order to avoid rendering artifacts that are caused by partial occlusions, which are most visible at silhouettes of objects in sub-images (Barsky et al., 2005). This is achieved by only increasing the opacity of pixels as described in this section.

The opaque blur of an RGBA image consists of three steps, which are illustrated in Figure 3.

1. A glow filter (James and O’Rourke, 2004) is applied to the A channel of the RGBA image (Figures 3b and 3d). This glow filter must not decrease the A channel of any pixel. The result is called  $A_{glow}$ .
2. A standard blur filter is applied to all channels of the original RGBA image (Figures 3a and 3c). The result is called  $RGBA_{blur}$ .
3. The opacity of the blurred image is replaced by the opacity computed by the glow filter

(Figure 3e). To this end, the blurred colors are rescaled since they are considered opacity-weighted colors. The result is called  $RGBA_{sub}$ :

$$RGBA_{sub} \stackrel{\text{def}}{=} RGBA_{blur} \times \frac{A_{glow}}{A_{blur}} \quad (7)$$

For each sub-image of the algorithm described in Section 3, the result  $RGBA_{sub}$  is then used in Equation 6.

Without the color rescaling, the increased opacity  $A_{glow}$  would result in dark silhouettes around objects of full opacity. To avoid artifacts, the range of the glow filter should not be larger than the range of the blur filter. Otherwise, the color rescaling is likely to increase colors that are unrelated to the objects that caused the increased opacity.

While any non-decreasing glow filter and any standard blur filter can be used to implement an opaque image blur, we propose to employ pyramid algorithms for both filters because of their favorable performance on GPUs. Moreover, pyramid versions of the glow filter and the blur filter can share a common analysis phase, which reduces the total computational costs by about one quarter.

For the standard blur we employ a pyramidal blur (Strengert et al., 2006) with a  $4 \times 4$  box analysis filter (Kraus and Strengert, 2007b). The analysis phase of this pyramidal blur corresponds to a mipmap generation; however, the number of required levels is limited by the strength of the blur. For the algorithm discussed in Section 3,  $|i|$  levels of the image pyramid have to be computed for the  $i$ -th sub-image. The synthesis phase of the pyramidal blur iteratively expands the  $i$ -th pyramid level to the original size with a synthesis filter that corresponds to a biquadratic B-spline interpolation (Strengert et al., 2006).

The glow filter makes use of the opacity  $A_{ana}$  of the exact same analysis pyramid as the pyramidal blur. However, the synthesis is modified in order to guarantee that the opacity of no pixel is decreased. This is achieved by multiplying the transparency of each expanded level, i.e.,  $1 - A_{exp}$ , with the transparency of the corresponding analysis level of the same size, i.e.,  $1 - A_{ana}$ . The resulting transparency determines the opacity  $A_{syn}$  of the new synthesis level for the pyramidal glow:

$$A_{syn} \stackrel{\text{def}}{=} 1 - (1 - A_{exp})(1 - A_{ana}) \quad (8)$$

$$= A_{exp} + A_{ana} - A_{exp}A_{ana}. \quad (9)$$

It is straightforward to implement this blending in a fragment shader.

After both pyramid algorithms have been performed, the blurred colors have to be rescaled to the opacity computed by the glow filter as discussed

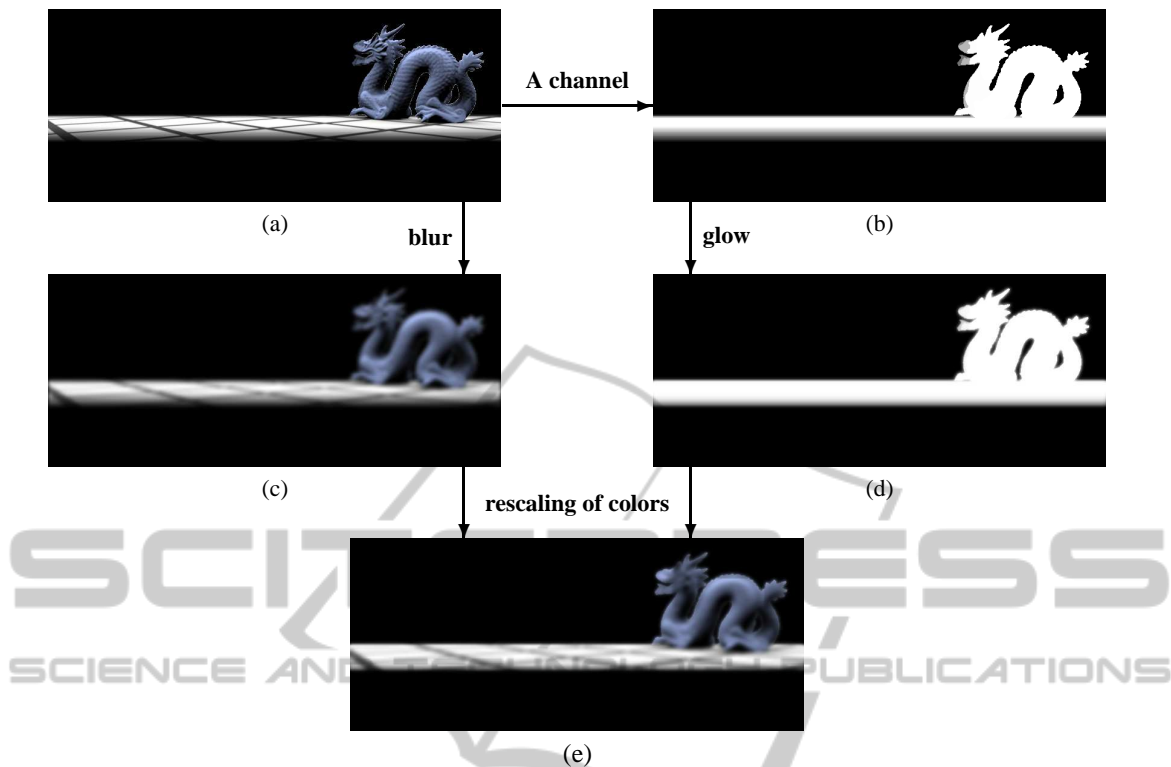


Figure 3: Data flow in the opaque image blur: (a) input RGBA image (only RGB is shown), (b) opacity (i.e., A channel) of the input image visualized as gray-scale image, (c) standard blur filter applied to the input RGBA image (A is not shown), (d) glow filter applied to the opacity of the input image, (e) resulting opaque image blur.

above. For efficiency, this step should be combined with the final synthesis step of the pyramidal blur and the final synthesis step of the pyramidal glow. Since the final synthesis steps expand the image to the full size of the input image, it is particularly beneficial to implement these steps as efficiently as possible.

## 5 RESULTS

Figure 4 compares two images generated by our method with ray-traced images computed with pbrt (Pharr and Humphreys, 2004) and images produced by the method proposed by Kraus and Strengert. Obviously, our method avoids any disocclusion which results in too opaque objects. On the other hand, color bleeding between objects at different depths is still avoided. Due to the nonlinear glow, the silhouettes of objects are too sharp in our method. This is, however, a consequence of the particular glow filter employed in this work. We assume that there are alternative glow filters that produce better visual results.

Our method performed  $1.9\times$  faster than the

method by Kraus and Strengert on a 13" MacBook Pro with an NVIDIA GeForce 320M, i.e., almost twice as fast. While our implementation of both methods was not optimized and includes some copy operations that could be avoided, we don't see many possibilities to optimize the disocclusion part of the method by Kraus and Strengert; therefore, it is unlikely that we overestimate the improvement gained by avoiding the disocclusion.

The implementation also revealed an interesting side effect of our method: artifacts at the boundaries of the view port are effectively avoided by the opaque image blur if there is a border of transparent black pixels. In particular, a border width of one pixel is sufficient. In contrast, the system by Kraus and Strengert requires an embedding of the view port in a larger framebuffer and relies on extrapolation to generate pixel data that provides continuous blurring at the boundaries of the original view port.

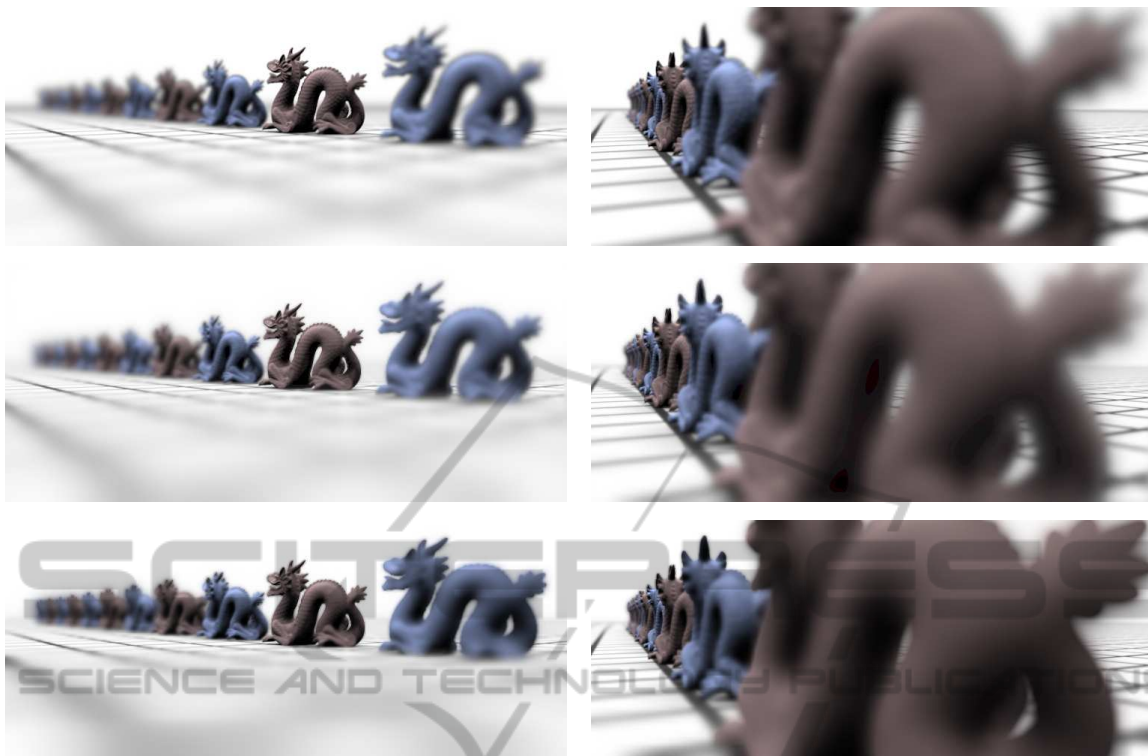


Figure 4: Comparison of renderings with depth of field generated by pbrt (Pharr and Humphreys, 2004) (*top row*), the method published by Kraus and Strengert (*middle row*), and the proposed method (*bottom row*).

## 6 CONCLUSIONS

The performance of the presented algorithm is independent of the scene complexity and independent of the rendering of the pinhole image. It offers a significantly improved performance in comparison to algorithms based on the blurring of sub-image (Barsky et al., 2005; Kraus and Strengert, 2007a) as it avoids the costly computations required by disocclusions of pixels. Moreover, our algorithm is easier to implement since algorithms for the disocclusion of pixels tend to be rather complex. On the other hand, the performance of our method is worse than methods based on computing differently blurred versions of a pinhole image (Hammon, 2007; Lee et al., 2009b).

The image quality achieved by the proposed algorithm is also between these two approaches: it avoids artifacts such as color bleeding between objects of different depths, which often occur in methods that do not use sub-images (Hammon, 2007; Lee et al., 2009b). On the other hand, the image quality is reduced in comparison to other approaches based on sub-images (Barsky et al., 2005; Kraus and Strengert, 2007a) because of the missing disocclusions and the particular opaque image blur.

In summary, we propose a new depth-of-field ren-

dering algorithm with a unique trade-off between performance and image quality. Maybe even more importantly, this work demonstrates a new technique to handle disocclusions in depth-of-field rendering. To this end, an “opaque image blur” has been proposed, which might find further applications apart from depth of field as discussed in the next section.

## 7 FUTURE WORK

Future work includes research on alternative glow filters for the opaque image blur described in Section 4. Of particular interest are glow filters that result in convincing depth-of-field effects.

Further potential applications of the opaque image blur include the application of motion blur and generalized depth-of-field effects (Kosloff and Barsky, 2007) to arbitrary parts of bitmap images. In these cases, some parts of an image have to be blurred without any information about the disoccluded pixels. Since the opaque image blur avoids the disocclusion of pixels, it offers an extremely efficient alternative to more costly disocclusion techniques.

## REFERENCES

- Barsky, B. A. (2004). Vision-realistic rendering: Simulation of the scanned foveal image from wavefront data of human subjects. In *APGV '04: Proceedings of the 1st Symposium on Applied Perception in Graphics and Visualization*, pages 73–81.
- Barsky, B. A., Tobias, M. J., Chu, D. P., and Horn, D. R. (2005). Elimination of artifacts due to occlusion and discretization problems in image space blurring techniques. *Graphical Models*, 67(6):584–599.
- Cook, R. L., Carpenter, L., and Catmull, E. (1987). The Reyes image rendering architecture. In *SIGGRAPH '87: Proceedings of the 14th Annual Conference on Computer Graphics and Interactive Techniques*, pages 95–102.
- Cook, R. L., Porter, T., and Carpenter, L. (1984). Distributed ray tracing. In *SIGGRAPH '84: Proceedings of the 11th Annual Conference on Computer Graphics and Interactive Techniques*, pages 137–145.
- Demers, J. (2004). Depth of field: A survey of techniques. In Fernando, R., editor, *GPU Gems*, pages 375–390. Addison Wesley.
- Haerberli, P. and Akeley, K. (1990). The accumulation buffer: hardware support for high-quality rendering. In *SIGGRAPH '90: Proceedings of the 17th annual conference on Computer graphics and interactive techniques*, pages 309–318. ACM.
- Hammon, E. (2007). Practical post-process depth of field. In Nguyen, H., editor, *GPU Gems 3*, pages 583–606. Addison Wesley.
- James, G. and O'Rorke, J. (2004). Real-time glow. In Fernando, R., editor, *GPU Gems*, pages 343–362. Addison Wesley.
- Kolb, C., Mitchell, D., and Hanrahan, P. (1995). A realistic camera model for computer graphics. In *SIGGRAPH '95: Proceedings of the 22nd annual conference on Computer graphics and interactive techniques*, pages 317–324. ACM.
- Kosloff, T. J. and Barsky, B. A. (2007). An algorithm for rendering generalized depth of field effects based on simulated heat diffusion. In *ICCSA'07: Proceedings of the 2007 international conference on Computational science and its applications*, pages 1124–1140.
- Kosloff, T. J., Tao, M. W., and Barsky, B. A. (2009). Depth of field postprocessing for layered scenes using constant-time rectangle spreading. In *Proceedings of Graphics Interface 2009, GI '09*, pages 39–46.
- Kraus, M. and Strengert, M. (2007a). Depth-of-field rendering by pyramidal image processing. *Computer Graphics forum (Proceedings Eurographics 2007)*, 26(3):645–654.
- Kraus, M. and Strengert, M. (2007b). Pyramid filters based on bilinear interpolation. In *Proceedings GRAPP 2007 (Volume GM/R)*, pages 21–28.
- Křivánek, J., Žára, J., and Bouatouch, K. (2003). Fast depth of field rendering with surface splatting. In *Proceedings of Computer Graphics International 2003*, pages 196–201.
- Lee, S., Eisemann, E., and Seidel, H.-P. (2009a). Depth-of-field rendering with multiview synthesis. *ACM Transactions on Graphics (Proc. ACM SIGGRAPH ASIA)*, 28(5):1–6.
- Lee, S., Eisemann, E., and Seidel, H.-P. (2010). Real-time lens blur effects and focus control. *ACM Transactions on Graphics (Proc. ACM SIGGRAPH'10)*, 29(4):65:1–7.
- Lee, S., Kim, G. J., and Choi, S. (2008). Real-time depth-of-field rendering using splatting on per-pixel layers. *Computer Graphics Forum (Proc. Pacific Graphics'08)*, 27(7):1955–1962.
- Lee, S., Kim, G. J., and Choi, S. (2009b). Real-time depth-of-field rendering using anisotropically filtered mipmap interpolation. *IEEE Transactions on Visualization and Computer Graphics*, 15(3):453–464.
- Pharr, M. and Humphreys, G. (2004). *Physically Based Rendering: From Theory to Implementation*. Morgan Kaufmann Publishers Inc.
- Porter, T. and Duff, T. (1984). Compositing digital images. In *SIGGRAPH '84: Proceedings of the 11th annual conference on Computer graphics and interactive techniques*, pages 253–259. ACM.
- Potmesil, M. and Chakravarty, I. (1982). Synthetic image generation with a lens and aperture camera model. *ACM Trans. Graph.*, 1(2):85–108.
- Rokita, P. (1993). Fast generation of depth of field effects in computer graphics. *Computers & Graphics*, 17(5):593–595.
- Scofield, C. (1992). 2 1/2-d depth-of-field simulation for computer animation. In *Graphics Gems III*, pages 36–38. Academic Press Professional.
- Shinya, M. (1994). Post-filtering for depth of field simulation with ray distribution buffer. In *Proceedings of Graphics Interface '94*, pages 59–66.
- Sternberg, S. (1986). Grayscale morphology. *Computer Vision, Graphics, and Image Processing*, 35(3):333–355.
- Strengert, M., Kraus, M., and Ertl, T. (2006). Pyramid methods in GPU-based image processing. In *Proceedings Vision, Modeling, and Visualization 2006*, pages 169–176.